ACS APPLIED MATERIALS & INTERFACES

Research Article

www.acsami.org

Highly Aging-Resistant Elastomers Doped with Antioxidant-Loaded Clay Nanotubes

Ye Fu,[†,‡] Detao Zhao,[†,‡] Pengjun Yao,[†] Wencai Wang,*[,†,‡] Liqun Zhang,*[,†,‡] and Yuri Lvov*[,§]

[†]State Key Laboratory of Organic−Inorganic Composites and [‡]Key Laboratory of Beijing City on Preparation and Processing of Novel Polymer Materials, Beijing University of Chemical Technology, Beijing 100029, China

[§]Institute for Micromanufacturing, Louisiana Tech University, Ruston, Louisiana 71270, United States

Supporting Information

ABSTRACT: A novel aging-resistant styrene−butadiene rubber (SBR) composite is prepared using the antioxidant *N*-isopropyl-*N*′-phenyl-p-phenylenediamine (4010NA) loaded inside of halloysite clay nanotubes and used as filler. Loading the antioxidant inside of halloysite allows for its sustained release for nine months in the rubber matrix. By utilizing modified halloysite, the antioxidant concentration in this rubber nanoformulation is tripled without causing "blooming" defects. Furthermore, the halloysite is silanized to enhance its miscibility with rubber. The aging resistance of SBR−halloysite composites is studied by comparing the mechanical properties before and after thermal-oxidative aging. A seven-day test at 90 °C shows preservation of mechanical properties, and no 4010NA blooming is observed, even after one month. Styrene−butadiene rubber with 27 wt % halloysite loaded with 4010NA shows marked increase in aging resistance and promising future of halloysite as a functional rubber filler.

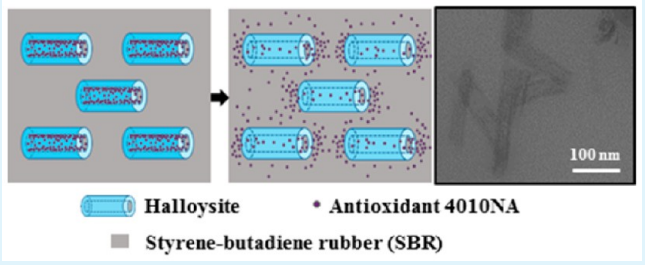

KEYWORDS: *Aging resistant, elastomer, sustained release, nanotubes, halloysite*

1. INTRODUCTION

Elastomer aging is caused by high temperature, oxygen, oil, acids, alkali, and other active chemicals. This process leads to deterioration of the chemical and mechanical properties of the rubber and makes it less elastic, harder, and mechanically unstable.[1−4] Because thermal-oxidative aging is the most common type of rubber aging, chemical antioxidants are added into elastomer compounds to extend the lifetime of the product by binding with oxygen/ozone. Maintaining a supply of antioxidants in bulk rubber is important; however, antioxidants often diffuse toward the surface of rubber products in an event called "blooming". Blooming results in microdefects, loss of antioxidant protection, and contaminates the environment.[5,6] Because of these issues, only about 1 wt % antioxidant can be added to an elastomer formulation, which does provide limited aging resistance and is not high enough to elicit blooming.[7−9] A polymeric encapsulation of rubber additives and some microencapsulation that can be used for the antiblooming formulation have been performed.[10−15] However, the sustained release of antioxidant for the antiblooming aging resistant elastomer composites has not been published.

Halloysite tubes are an economically viable aluminosilicate clay with a hollow cylindrical structure in the submicron range. Halloysite is mined from natural deposits as a raw material (white stones resembling chalk), and are then milled and heated to 110−120 °C to remove hydrated water (providing tighter wall packing with layer periodicity shifting from 1.0 to 0.7 nm). Halloysite is available in thousands of tons at low prices from a number of companies in the United States, New Zealand, China, and Turkey. Halloysite may be considered as a rolled sheet of kaolin containing 15−20 internal layers. Halloysite tubes are 50−70 nm in diameter, have a 10−15 nm lumen, and are ca. 1 μm long. The surface of halloysite is comprised of SiO_2 and its internal lumen is Al_2O_3. It is possible to load the lumen of the tube with inhibitors such as anticorrosion, flame retardant, and antimicrobial agents and enable halloysite to be a functional filler for polymers.[16−20] The halloysite loading capacity is 15−20 wt % and the loaded agents release from the tubes within hours to days if these nanotubes are dispersed in solutions, and within months to years if the halloysite is embedded in a polymeric matrix.[21−25] All these advantages make halloysite an accessible nanocontainer for loading chemical inhibitors which allows for sustained release.

An important advantage of tubule halloysite when compared with platy clays such as montmorillonite, kaolin, and bentonite, which are stacked in larger crystallites, is that it does not need exfoliation.[18,26] Rubber nanocomposites with fibrillar and tubular clay have attracted a lot of attention due to the significant reinforcing effect and decreased permeability compared with those that have conventional spherical fillers.[21,27−30] Halloysite can be easily dispersed in water or polar polymers. Surprisingly, halloysite is also well dispersed in low

Received: February 2, 2015
Accepted: March 25, 2015
Published: April 8, 2015

DOI: 10.1021/acsami.5b00993
ACS Appl. Mater. Interfaces 2015, 7, 8156−8165

polar polymers and even in melted polypropylene. Under the strong shearing force of the blending process, surface silanized halloysite have much weaker interactions among their single nanoparticles forms, even nanodispersions in bulk rubber.[31,32] Tight interfacial bonding and fine dispersions of the clay are crucial factors for the best performance of the styrene−butadiene rubber/halloysite composites.[33] After endowing these tubular nanofillers with different functions, they can be used for elastomer reinforcement while exhibiting synergy in physical and chemical properties of the matrix and filling materials.

In this work, loading halloysite nanotubes with *N*-isopropyl-*N*′-phenyl-p-phenylenediamin (antioxidant 4010NA) and filling them at 27 wt % into styrene−butadiene rubber (SBR) allowed for sustained release during nine months, providing rubber aging protection. The release kinetics of 4010NA from halloysite in water, nonpolar solvent (cyclohexane), and bulk rubber was analyzed for the composition optimization. The aging resistance of SBR/HNTs composites was studied by comparing the mechanical properties before and after thermal-oxidative aging. The antioxidant-loaded halloysite allowed tripling the antioxidant amount in the composite without blooming, thus providing an excellent antiaging protection demonstrated with the retention of the mechanical properties after aging for 7 days at 90 °C.

2. EXPERIMENTAL SECTION

2.1. Materials. Halloysite was obtained from Applied Minerals Inc., USA. Styrene−butadiene rubber (SBR), with trademark SBR1502 (styrene content 23.5 wt %), was manufactured by Jilin Chemical Industry Company, China. Silane coupling agent KH570 (3-(methacryloyloxy)propyltrimethoxysilane) was from Nanjing Shuguang Chemicals Co., Ltd. Zinc oxide (ZnO) was analytical grade from Sigma-Aldrich, USA. Antioxidant *N*-isopropyl-*N*′-phenyl-p-phenylenediamine (4010NA) was from SINOPEC Nanjing Chemical Industries Co., Ltd. Other rubber additives, including steartic acid, sulfur, 2-mercaptobenzothiazole, diphenyl guanidine, and tetramethyl thiuram disulfide, were industrial grade and used as received and without further purification.

2.2. Preparation of Antioxidant 4010NA-Loaded HNTs. Halloysite (60 g/L) was mixed thoroughly with antioxidant acetone solution (30 g/L) and placed in a vacuum chamber at 100 Torr for 30 min, then at atmospheric pressure for 15 min. This vacuum cycle was repeated three times, followed by washing with deionized (DI) water to remove any unloaded antioxidant. Samples were placed in a vacuum oven at 50 °C for drying. The dried antioxidant 4010NA-loaded halloysite samples (HNTs−4010NA) were milled to a fine powder.

2.3. Preparation of the SBR/HNTs Nanocomposites. Halloysite was first modified by silane coupling agent (KH570). Specifically, the modification was made by dispersing halloysite into DI water (50 wt %), adding KH570 with stirring during 30 min at 60 °C, followed with centrifugation, drying, and grinding. The mass rate of KH570 to halloysite was 0.05.

SBR and KH570-modified halloysite were compounded with rubber additives using a two-roll mill at room temperature. The compositions of the rubber compounds are tabulated in Table 1. The compound was press-cured to a 1-mm-thick sheet at 150 °C × Tc90 and then cut into specimens.

2.4. Characterization. Thermogravimetric analysis (TGA) of antioxidant loaded halloysite was performed on a TGA-60A (Shimadzu, Japan) from 30 to 600 °C at a rate of 10 °C/min with a steady nitrogen flow (50 mL/min).

Scanning electron microscopy (SEM) was performed on a Hitachi S-4800 scanning electron microscope (Hitachi, Japan). The surface of the sample was sputtered with a thin layer of gold prior to the measurements. The SEM measurements were performed at an accelerating voltage of 5 kV and 20 kV. Energy dispersive spectrometry (EDS) was performed on an HORIBA X-Max20 detector (Japan) attached to the scanning electron microscope.

Table 1. Composition of SBR/HNTs Nanocomposites[a]

sample code	SBR	halloysite (phr)	HNTs−4010NA (phr)	4010NA (phr)
SBR#1	100			
SBR#2	100	40 (27 wt %)		
SBR#3	100			1.5 (1.0 wt %)
SBR#4	100		40 (27 wt %)	
SBR#5	100		40 (27 wt %)	1.5 (1.0 wt %)

[a]Rubber ingredients: zinc oxide, 5 phr (parts per hundred rubber); stearic acid, 1 phr; sulfur, 2 phr; accelerator (2-mercaptobenzothiazole, 0.5 phr; diphenyl guanidine, 0.5 phr; tetramethyl thiuram disulfide, 0.2 phr).

Transmission electron microscopy (TEM) images were recorded on FEI Taicnai G2 20 STWIN TEM at 200 kV. Halloysite specimens were dropped onto carbon support films on a copper grid, and the solvent was allowed to evaporate before observation. The ultrathin section specimens of SBR/HNTs for TEM observation were cut with a diamond knife on Cro-Ultramicrotome (Leica EM UC6, Germany). HR-TEM was performed on a JEM-3010 electron microscope (JEOL, Japan) with an acceleration voltage of 300 kV.

The chemical structure of halloysite was characterized by Fourier transform infrared spectroscopy (FTIR). FTIR spectra were obtained by using a TENSOR 27 spectrometer under ambient conditions. The test samples were prepared by uniform dispersion in KBr and pressing the powder into pellets.

The change in hydrophobicity of halloysite was characterized by static water contact angle at 25 °C and 50% relative humidity by the sessile drop method using a 2-μL water droplet in a telescopic goniometer (OCA15EC, Dataphysics, Germany). The halloysite pellet was obtained by pressing in a mold under 10 MPa for about 3 min at room temperature. For each sample, 15 measurements from different surface locations were averaged.

Ultraviolet visible spectrophotometry (UV−vis) was carried out with Spectrophotometer Agilent 8453 (Agilent Technology, 2012). The UV−vis was used to analyze kinetics of antioxidant release both in water and cyclohexane. Antioxidant release experiments were conducted by stirring 50 mg of 4010NA-loaded halloysite in 1 mL of DI water or cyclohexane. At each reading, the supernatant was removed by centrifugation and fresh solvent was added. The collected supernatant was analyzed by UV−vis spectroscopy at 285 nm for the amount of 4010NA.

The vulcanization characteristics of the SBR compounds were determined at 150 °C by rotorless rheometer MR-C3 (RAD Co., Ltd., Beijing, China). The cross-linking density was determined with the XLDS-15 Polymer/Rubber Cross-link Density Analyzer and NMR Spectrometer (IIC Innovative Imaging Corp. KG, Germany).

X-ray photoelectron spectroscopy (XPS) measurements were carried out on an ESCALAB 250 XPS system (Thermo Electron Corporation, USA) with an Al Kα X-ray source (1486.6 eV photons). The core-level signals were obtained at a photoelectron takeoff angle of 45° with respect to the sample surface. The X-ray source was run at a reduced power of 150 W. The samples were mounted on standard sample studs by means of double-sided adhesive tape. The pressure in the analysis chamber was maintained at 10^{-8} Torr.

Tensile tests of dogbone specimens were performed with a tensile apparatus (CMT4104, Shenzhen SANS Testing Machine Co., Ltd., China) at 25 °C according to Chinese Standard GB/T528-2009. The crosshead speed was 200 mm/min. For each sample, five measurements from different specimens were averaged.

3. RESULTS AND DISCUSSION

3.1. Antioxidant 4010NA Loading into Halloysite Lumens and Its Release Kinetics. The morphology of halloysite observed with scanning electron microscopy (SEM)

DOI: 10.1021/acsami.5b00993
ACS Appl. Mater. Interfaces 2015, 7, 8156−8165

and transmission electron microscopy (TEM) shows the high aspect ratio of length/diameter ~ 30 and the lumens with the diameter of 10−15 nm. The unique structure of halloysite makes it a promising nanocontainer (Figure 1).

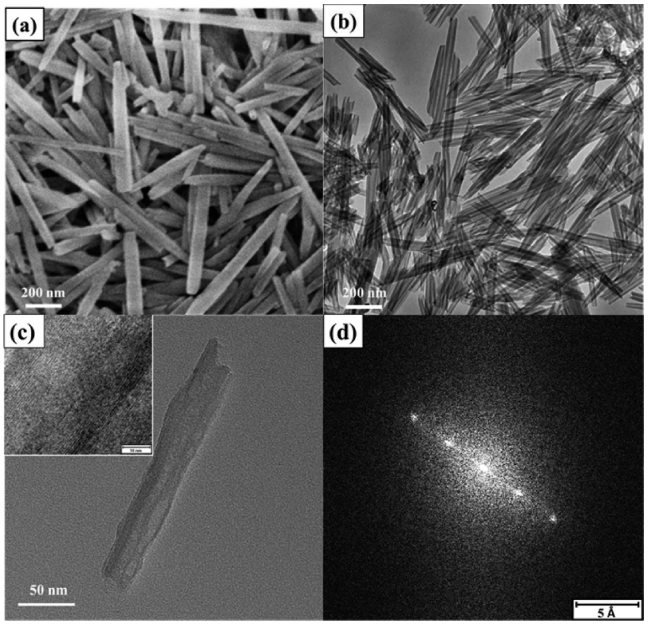

Figure 1. (a) SEM and (b) TEM images of halloysite nanotubes; (c) TEM image and HR-TEM of silane-modified antioxidant-loaded halloysite; (d) Fourier Transform of HR-TEM wall image from the inset.

Halloysite was exposed to concentrated solution of antioxidant in acetone. Then, air was removed from the tube lumens replacing it with antioxidant by cyclic application of vacuum and atmospheric air (Scheme 1).

To analyze the loading efficiency of antioxidant 4010NA, the weight loss of the samples prepared with different HNTs/4010NA weight ratios was measured by thermogravimetric

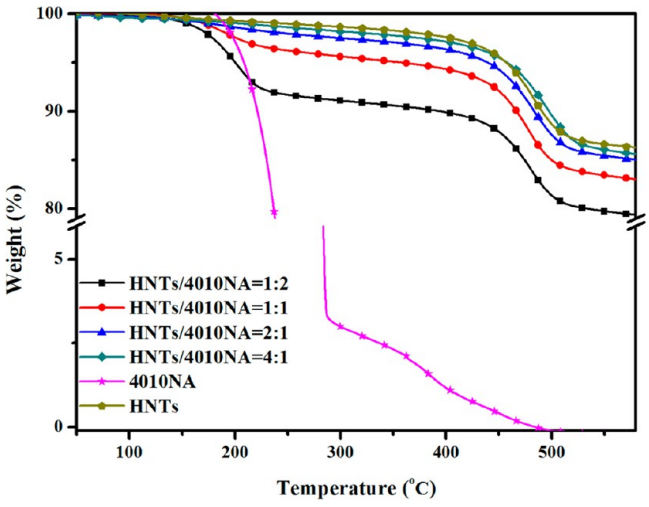

Figure 2. TGA curves of HNTs−4010NA prepared with different weight ratios of antioxidant in halloysite (antioxidant solution concentration was 5 wt %).

Scheme 1. Loading Procedure of Antioxidant into Halloysite and Surface Modification with Silane Coupling Agent

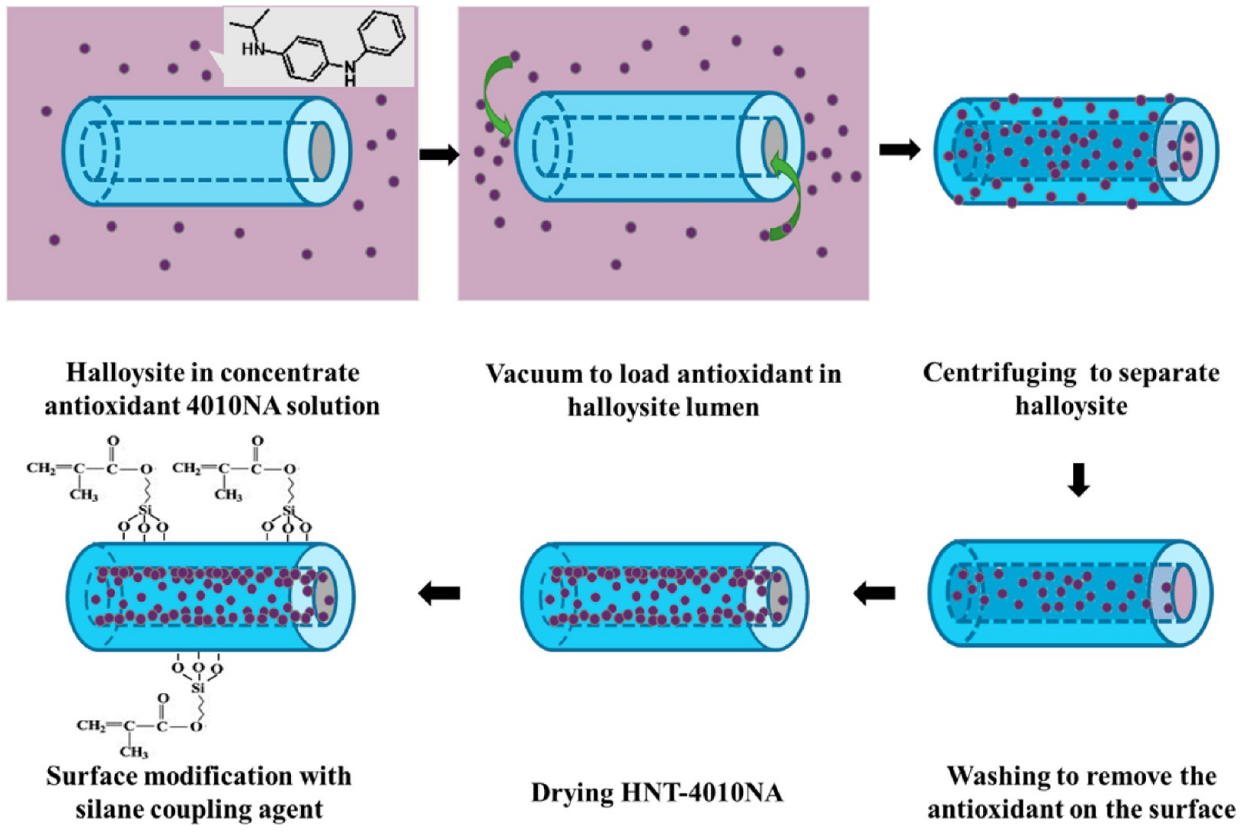

DOI: 10.1021/acsami.5b00993
ACS Appl. Mater. Interfaces 2015, 7, 8156−8165

analysis (TGA) (Figure 2). The loading efficiency calculated with eq 1 is listed in Table 2.

$$c_A = (1 - w_{H-A}/w_H) \times 100\% \quad (1)$$

Table 2. Loading Efficiency of HNTs−4010NA

	4:1	2:1	1:1	1:2
loading efficiency (wt %)	0.8	1.5	3.8	8.1

where c_A is the loading efficiency of antioxidant; w_{H-A} is the weight of antioxidant-loaded halloysite at 600 °C; and w_H is the weight of halloysite at 600 °C.

The loading efficiency increases with the increasing antioxidant in HNTs−4010NA until its maximum 8.1 wt % loading was achieved.

The morphology of silane-modified antioxidant-loaded halloysite (Figure 1c) shows that during the process halloysite does not change its tubular structure. In the inset image of Figure 1c, a periodic multilayer nature of the halloysite wall is shown. Periodicity in the individual layer packing was determined with the Fourier transform of the TEM image of the halloysite wall (Figure 1d), and gives two reflection orders corresponding to a multilayer with the periodicity of 0.69 ± 0.02 nm which is consistent with X-ray analysis of dehydrated halloysite.[34] This proves that antioxidant does not intercalate into the multilayer walls.

To further investigate the formation mechanism of the 4010NA loaded halloysite, we have compared the Fourier transform infrared spectroscopy (FT-IR) spectra (Figure 3) of

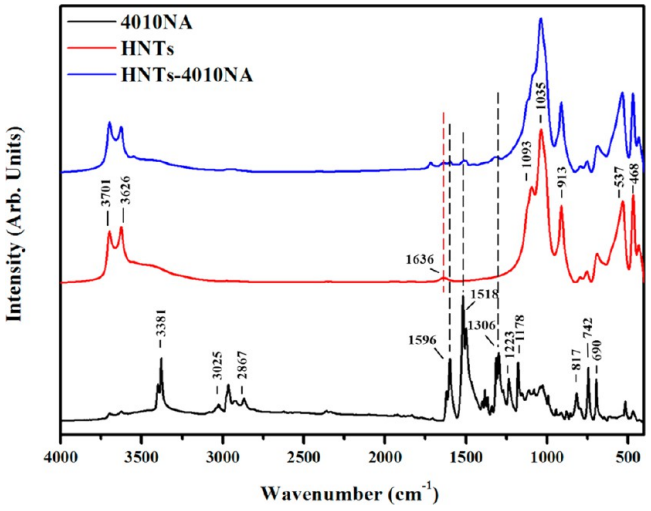

Figure 3. FT-IR spectra of antioxidant 4010NA, halloysite (HNTs), and 4010NA-loaded halloysite (HNTs−4010NA).

the pristine halloysite and 4010NA with those of the 4010NA-loaded halloysite. In the FT-IR spectrum of 4010NA, strong vibration bands observed at 1596 and 1518 cm^{-1} are ascribed to the combination of secondary amine flexure and aromatic rings. A series of vibrations in the region of 3025−2867 cm^{-1} is assigned to the symmetric and antisymmetric stretching vibration of $-CH_3$ and $-CH_2-$. The vibration ascribed to the stretching of secondary amine appears at 3381 cm^{-1}, while the band at 1223 cm^{-1} assigned to the stretching of C−N can be observed. The band at 1306 cm^{-1} assigned to the flexural vibration of $-CH_2-$ is enhanced by the double-bond feature of C−N which is attributed to the conjugate of the nitrogen lone pair electrons and benzene ring. The vibration that appeared at 817 cm^{-1} is ascribed to the flexure of the two adjacent C−H in the para-disubstituted benzene, while the vibration at 742 cm^{-1} is ascribed to the flexure of the five adjacent C−H in the monosubstituted benzene.

In the FT-IR spectrum of halloysite, the bands at 3701 and 3626 cm^{-1} are attributed to the stretching vibrations of inner-surface hydroxyl groups. Inter-layer water is demonstrated by the deformation vibration at 1636 cm^{-1}. The band at 1093 cm^{-1} is assigned to stretching vibration of apical Si−O, and the band at 1035 cm^{-1} is assigned to the stretching vibration of Si−O−Si. The band observed at 913 cm^{-1} is caused by the presence of intersurface hydroxyl groups. The vibrations ascribed to the Al−O−Si and Si−O−Si, respectively, at 554 and 469 cm^{-1} can further confirm the existence of corresponding group. When the halloysite was loaded with antioxidant 4010NA, the vibrations of 4010NA such as those at 1596, 1518, and 1306 cm^{-1} appeared, indicating the loading of 4010NA, while the band at 1636 cm^{-1} of the halloysite inter-layer water kept its shape. This indicates the loading of antioxidant is a physical process and there is no chemical reaction between antioxidant and halloysite.

Ultraviolet visible spectrophotometry (UV−vis) was used to analyze kinetics of antioxidant release from halloysite both in water and cyclohexane. The release of antioxidant in cyclohexane was much faster than in water (3 and 6 h), attributed to its higher solubility in cyclohexane (Figure 4a). The antioxidant release bust at the initial stage is acceptable for the rubber protection initiation.

However, of practical importance is the antioxidant release from nanotubes embedded in rubber. The release in rubber is drastically slowed down as the halloysite openings are clogged with the cross-linked rubber. The release speed is affected by the viscosity of medium and its affinity with antioxidant. The release of antioxidant from halloysite in rubber composite was calculated with eq 2. The element amount is obtained with the energy dispersive spectrometry (EDS) measurement. As there is no nitrogen in the composite without antioxidant and nor silicon without halloysite, the amount of antioxidant and halloysite in the view area can be calculated with the amount of nitrogen and silicon.

$$R = \left(m_H - \frac{m_N \cdot (1 - c_A)}{w_{N-A}}\right) / (m_H - w_{H-C} \cdot (1 - c_A)) \quad (2)$$

where m_H is the amount of halloysite in the EDS view area, $m_H = (m_{Si}/(w_{Si-H}))$, where w_{Si-H} is the weight ratio of silicon in halloysite, w_{Si-H} = 22.6%; m_N is the N element amount of the rubber composite in the EDS view area; C_A is the loading efficiency of antioxidant; w_{N-A} is the weight ratio of N in antioxidant, w_{N-A} =12.4%; and w_{H-C} is the weight ratio of halloysite in SBR/HNTs composite, w_{H-C} = 27%.

The release kinetics of antioxidant from halloysite in rubber composite at 90 °C demonstrates slow and sustained release (Figure 4b). The release amount is 14.4% for 1 day and 90.2% for 18 days at 90 °C. The antioxidant release at room temperature (25 °C) from halloysite in SBR/HNTs composite was much slower: 7%, 11%, 21%, 39%, and 66% after 1.5, 2, 3, 4, and 5 months, making this rubber nanoformulation practically feasible (Figure 4c). An extrapolation allows estimating that 90% release will take 9 months.

DOI: 10.1021/acsami.5b00993
ACS Appl. Mater. Interfaces 2015, 7, 8156−8165

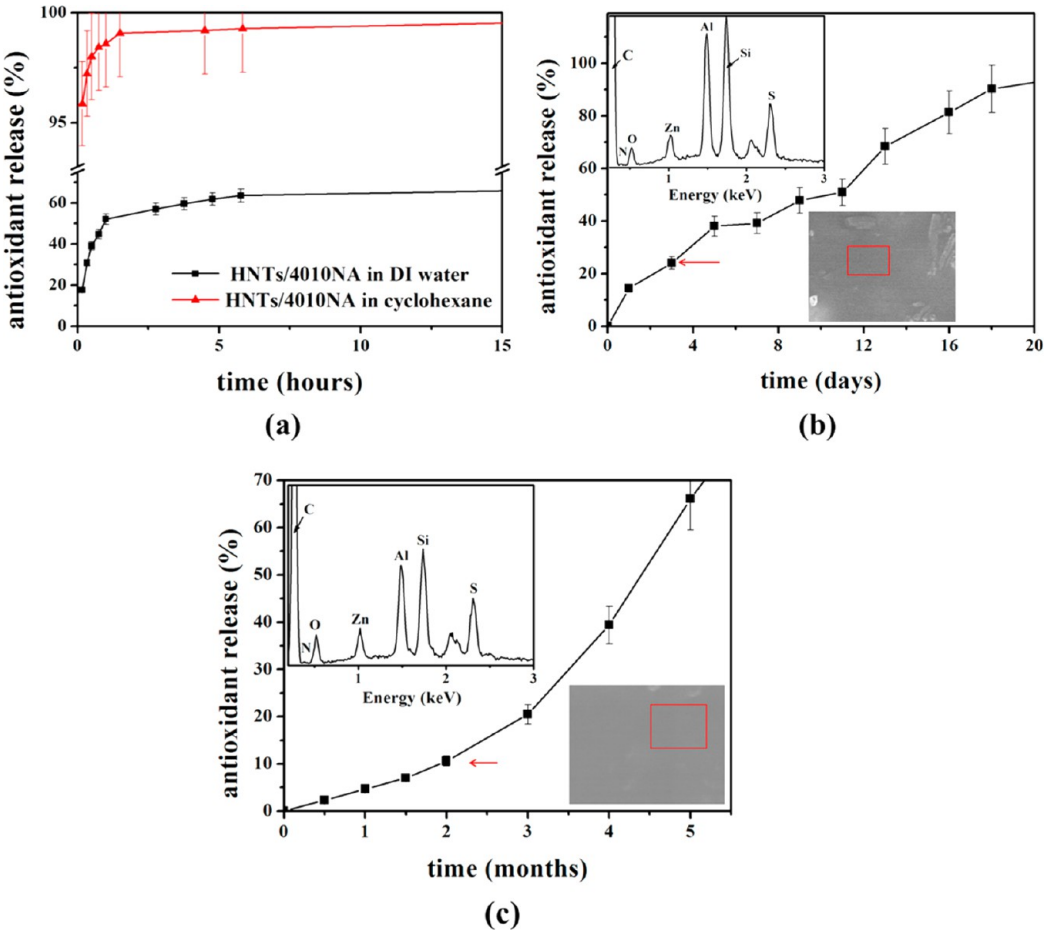

Figure 4. Antioxidant 4010NA release from (a) loaded halloysite in water and cyclohexane; halloysite rubber composite at (b) 90 °C and (c) 25 °C. The inset images are the SEM images and the EDS spectra of the selected area.

The water contact angles of pristine halloysite, silane modified halloysite, HNTs−4010NA, and silane-modified HNTs−4010NA were 0°, 16°, 69°, and 94°, respectively (Figure 5). The contact angle of 4010NA-loaded halloysite increase indicates that the antioxidant is present also on the tube surface making halloysite more hydrophobic and better mixable with SBR.

3.2. Morphology and Properties of the SBR/HNTs Nanocomposites. Three controlled samples, pure SBR rubber (SBR#1), SBR rubber with 27 wt % of empty halloysite filler (SBR#2), and SBR rubber without halloysite admixed with 1.0 wt % of 4010NA antioxidant (SBR#3), were investigated. These three samples are not able to provide slow nanopore-controlled 4010NA release.

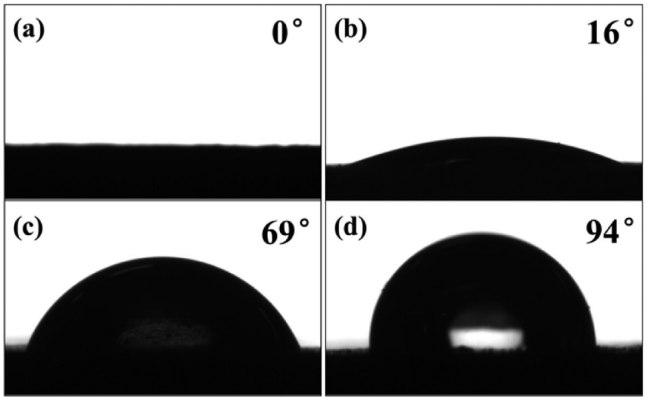

Figure 5. Water contact angle for halloysite tablet: (a) pristine halloysite, (b) silanized halloysite, (c) halloysite loaded with 4010NA, and (d) silane-modified antioxidant-loaded halloysite.

Two designed functional materials containing SBR filled with antioxidant-loaded halloysite (SBR#4) and the same material but with 1.0 wt % of free antioxidant added (SBR#5) also were investigated. They are given in the bottom two rows of Table 1. Therefore, in SBR#4 nanocomposite we had 2.2 wt % of nanotube encapsulated antioxidant and in SBR#5 we had 2.2 wt % of encapsulated 4010NA providing sustained release plus 1.0 wt % of 4010NA non-encapsulated antioxidant (blooming concentration threshold). With this formulation we tripled an amount of antioxidant agent dispersed in the rubber without blooming defects.

The morphology of these SBR/HNTs nanocomposites is shown in Figure 6. The dispersion of halloysite modified with silane was excellent (Figure 6b, c, d) which was not possible to achieve without such treatment. In the inset images, it is shown that the shape of nanotubes embedded into rubber matrix is preserved. We have to mention that with halloysite density of 2.53 g/cm^3, its 27 wt % filling corresponds to ca. 13 vol %, which is evident from the visual SEM image. The TEM images of SBR#2 (Figure 6e) and SBR#5 (Figure 6f) ultrathin sections show good halloysite tube dispersion in rubber matrix. Such an excellent dispersion of single clay particles was obtained

DOI: 10.1021/acsami.5b00993
ACS Appl. Mater. Interfaces 2015, 7, 8156−8165

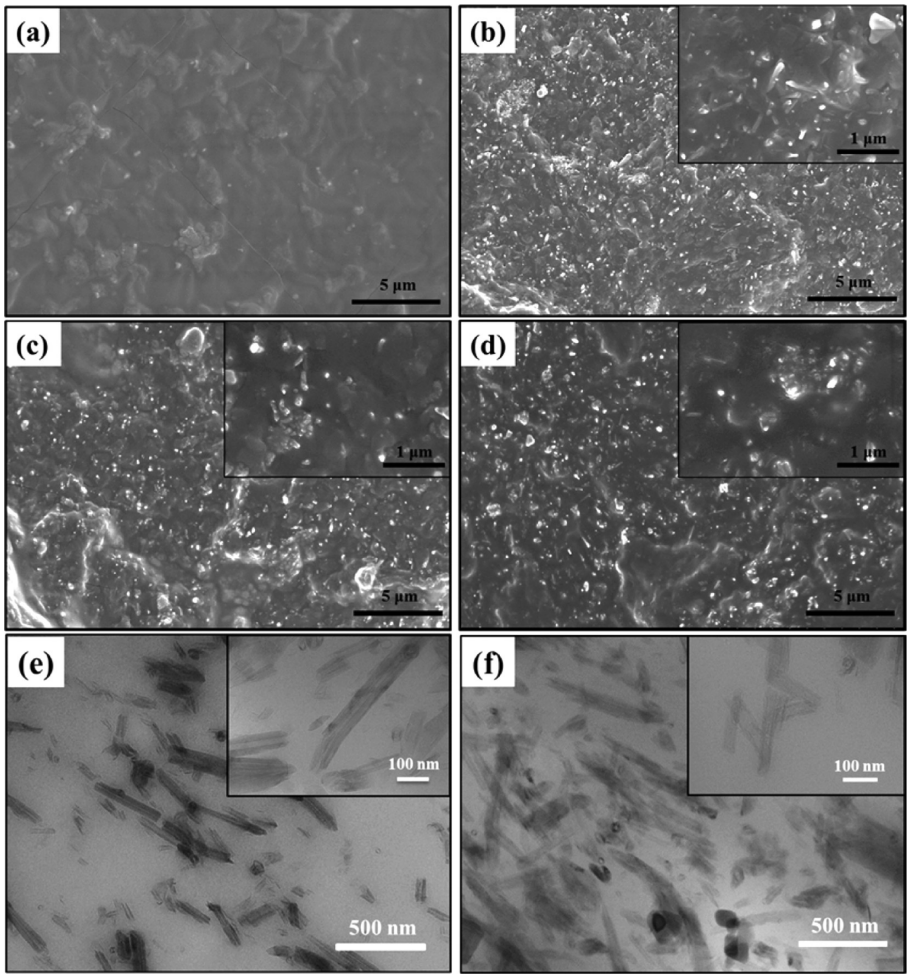

Figure 6. SEM images of SBR/HNTs composites with different formulas: (a) SBR#1 pure rubber, (b) SBR#2 pristine halloysite composites, (c) SBR#4 with 4010NA-loaded halloysite, and (d) SBR#5 with loaded halloysite plus admixed free antioxidant. TEM images of (e) SBR#2 and (f) SBR#5 ultrathin section surface.

without any additional exfoliation processing of this tubular clay.

The effect of antioxidant and HNTs on vulcanization and cross-linking density is described in Figure 7 and Table 3. In the target functional formulations (SBR#4 and SBR#5), the optimum curing time (T90) was reduced to 4 and 5 min. The inclusion of halloysite leads to significant increase of torque and curing rate index (CRI) of the vulcanization and the increase in cross-link density, which can be attributed to the silanized surface taking a part of cross-links and silane working as antireversion agent. Cross-linking density was enhanced 4−5% with halloysite filling. The cross-linking density of the composite with antioxidant (SBR#3, 4, 5) is slightly lower than the one without antioxidant because of antioxidant reacting with the free radicals; meanwhile, another reason could be the plasticization of antioxidant.

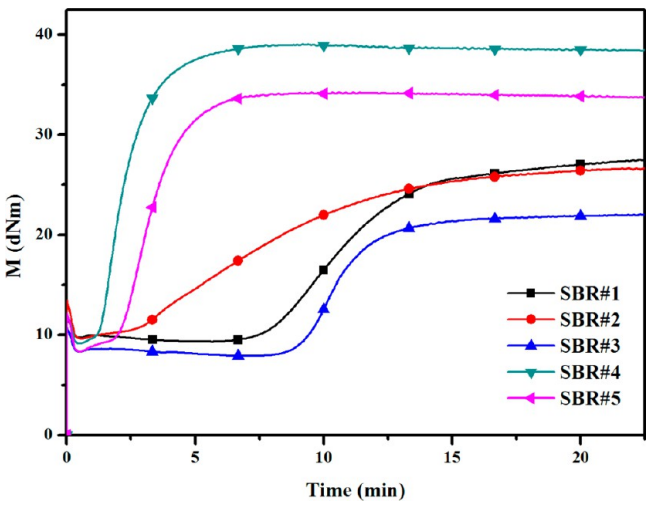

Figure 7. Vulcanization curves of the SBR/HNTs compounds.

3.3. Aging Performance of SBR/HNTs Nanocomposite.

The aging resistance of SBR/HNTs was studied by comparing the mechanical properties before and after thermal-oxidative aging. Figure 8 shows the mechanical properties of SBR/HNTs nanocomposites before and after aging at 90 and 120 °C for 24, 72, and 168 h.

Comparing with the SBR#1, the higher cross-linking density of the composite filled with pristine halloysite (SBR#2) leads to higher tensile strength, almost two-times. The hardness increases after the filling of halloysite that is attributed to its nano-reinforcement. The lower cross-linking density of composite with antioxidant (SBR#3 compared with SBR#1, SBR#4 compared with SBR#2, and SBR#4 compared with SBR#5) leads to higher elongation at break and lower hardness.

DOI: 10.1021/acsami.5b00993
ACS Appl. Mater. Interfaces 2015, 7, 8156−8165

Table 3. Cross-linking Density of SBR/HNT−1040NA Nanocomposite Samples

	SBR#1	SBR#2	SBR#3	SBR#4	SBR#5
cross-linking density/10^{-5}mol·cm^{-3}	14.96 ± 0.36	15.61 ± 0.47	14.35 ± 0.11	13.51 ± 0.17	14.69 ± 0.20

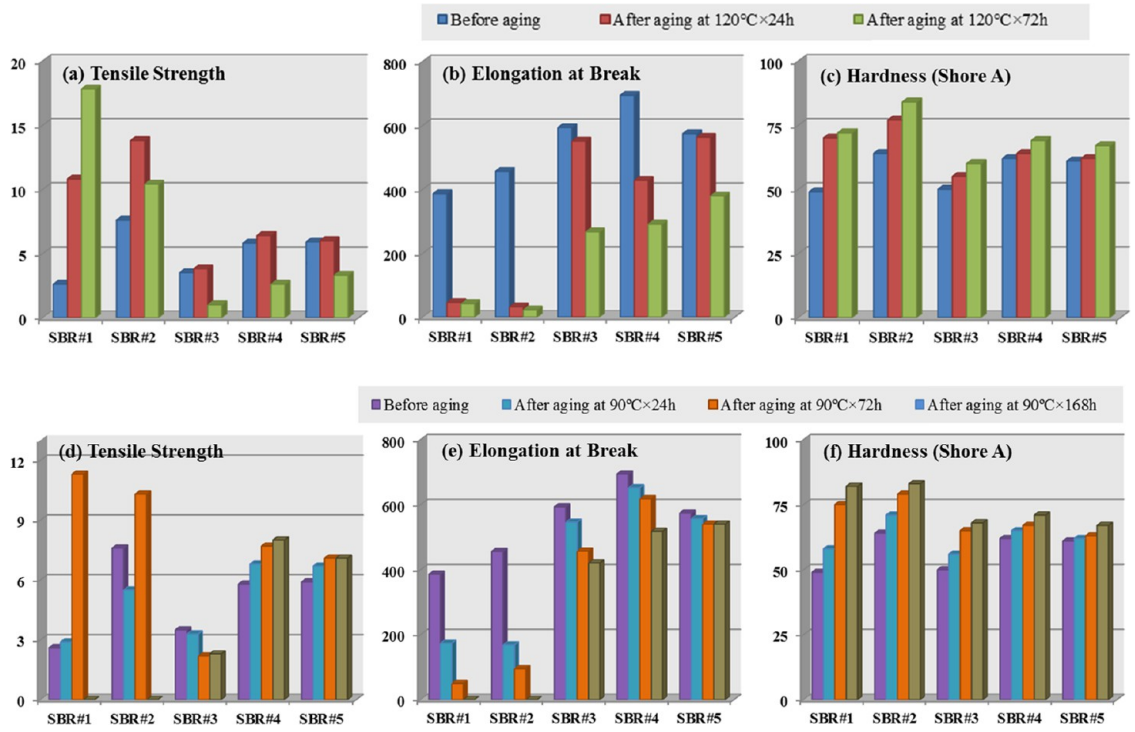

Figure 8. Mechanical properties of SBR/HNTs nanocomposites before and after aging at (a−c) 120 °C and (d−f) 90 °C (experimental error 5%).

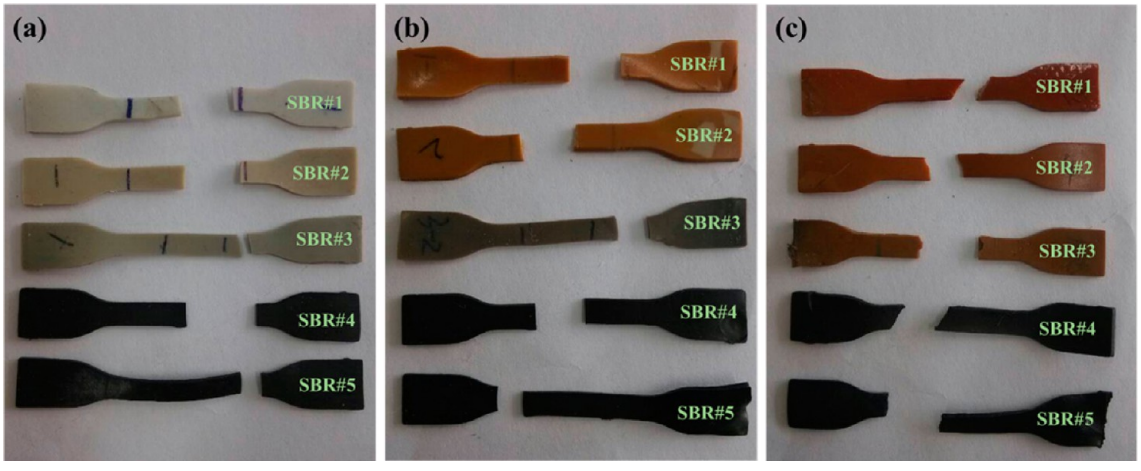

Figure 9. Images of tensile fracture dogbone-shaped rubber nanocomposite samples: (a) before aging, (b) after aging for 24 h, and (c) 168 h at 120 °C.

After aging for 24 h at 120 °C, the elongation at break of SBR#1 and with pristine halloysite filler (SBR#2) decreases significantly. Meanwhile, the retention rate of elongation at break of SBR#3 with the addition of antioxidant is at least 45% after aging for 72 h and the retention rate is 42% with the addition of HNTs−4010NA (SBR#4). The elongation at break is more or less the same even after aging for 168 h at 90 °C for the composite with the addition of both halloysite-encapsulated antioxidant and free antioxidant (our best sample SBR#5). This SBR#5 formulation demonstrates much better mechanical properties as comparing with direct loading of free antioxidant into rubber. The increase of hardness after aging is attributed to the further cross-linking of SBR, which leads to the loss of elasticity. SBR#5 containing 2.2 wt % of encapsulated plus 1.0 wt % of free antioxidant gave the least increase in hardness after 168 h aging, indicating great aging protection due to sustained release of antioxidant.

The SBR/HNTs composite enhanced mechanical properties demonstrate that HNTs−4010NA can not only take a role of reinforcing filler but also improve the aging resistance of this designed nanomaterial. Especially spectacular are results on 168 h aging at 90 °C when rubber without antioxidant became

DOI: 10.1021/acsami.5b00993
ACS Appl. Mater. Interfaces 2015, 7, 8156−8165

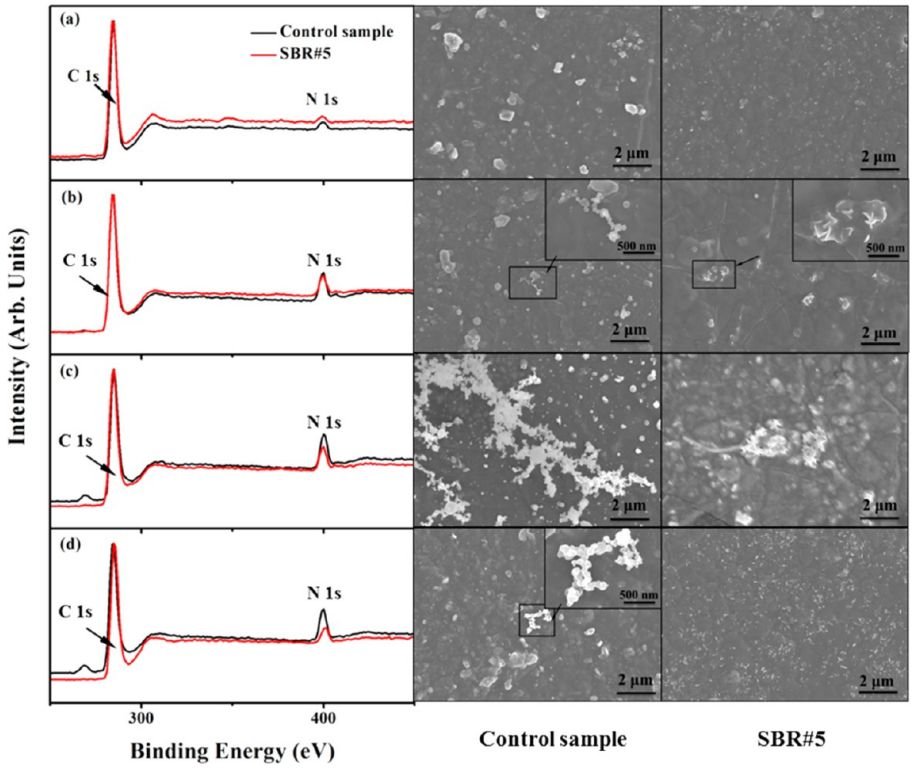

Figure 10. XPS wide scan spectra and the SEM images of the control samples and SBR#5 (a) before aging, and after aging for (b) 3 days, (c) 7 days, (d) 15 days.

brittle and just crashed at mechanical test, but sample SBR#5 with halloysite-encapsulated antioxidant demonstrated only 2% decrease in elongation break without losing tensile strength and elasticity (Figure 8e).

During the aging, formation and degradation of cross-links occur at the same time. If the formation is faster, the cross-linking density of composite will increase and the hardness will increase too, which leads to the decrease in the elasticity. The cross-linking density of SBR sample without filler or antioxidant (SBR#1) decreases with the aging time extended then increases. This is because at the initial stage the cross-links perform mild thermal degradation rather than further curing, which is the typical aging performance of polybutadiene (there is 76.5% of butadiene in the SBR we used). Thus, the tensile strength and elongation at break decrease, while the hardness increases. The changes in the cross-linking density of SBR with antioxidant (SBR#3, SBR#4, and SBR#5) are due to the free radical reaction with antioxidant instead of polymer molecules which slows down the further curing.

The photographs of tensile fracture dogbone-shaped samples before and after aging at 120 °C are shown in Figure 9. Without antioxidant, SBR#1 and SBR#2 turn yellow after 24 h aging and the color gets darker with longer aging time. For the sample of SBR#3, the gray color gets darker at the beginning of aging and finally turns to light brown at 168 h when antioxidant is exhausted.

The color retention of designed sample SBR#4 and SBR#5 with tube-encapsulated 4010NA indicates that sustained release of the antioxidant allows for long-lasting rubber protection while avoiding the blooming which otherwise would be inevitable at such high antioxidant content (3.2 wt %). After aging for 24 h, the permanent set at break of SBR#5 was the same with SBR#3 but the elongation at break of SBR#5 was much larger. This indicates that presence of 4010NA-loaded halloysite improved the sample elasticity.

3.4. Blooming Test of SBR/HNTs Nanocomposite As Compared with Direct Antioxidant Addition. The control sample for blooming test was prepared with addition of 27 wt % of empty halloysite plus 3.2 wt % free antioxidant, making its composition similar to the best sample SBR#5 but without antioxidant-loaded halloysite.

Keeping samples at 90 °C speeds up the blooming process. The blooming amount of antioxidant was analyzed with the nitrogen amount on the sample surface measured with XPS. The wide scan spectra after normalization show the much larger blooming amount of antioxidant on the surface of control sample than for the SBR#5 nanocomposite (Figure 10). The quantitative analysis indicates the nitrogen amount on the surface of control sample increases from 3.3 to 13.7 at. % after aging for 7 days then decreases to 12.0 at. % in 15 days, while the nitrogen amount on the surface of SBR#5 increases from 3.0 to 8.4 at. % after aging for 7 days then decreases to 4.8 at. % in 15 days. The results present the combined impact of the blooming and the antioxidant loss due to oxygen reaction and the vapor of antioxidant. The half-life of antioxidant is 3.5 days at 90 °C calculated with TGA data (Supporting Information (SI) Figure S1).

The SEM images of samples after the blooming test at 90 °C for 15 days are shown in Figure 10. The aggregates of antioxidant ("bloom") on the control sample surface were observed while one can see "clean" not blooming surface of the SBR#5 halloysite composite sample. The nitrogen amount of the aggregates is about 4 wt % measured with EDS (SI Figure S2) demonstrates the aggregates are antioxidant because there is no nitrogen except antioxidant. Thus, the amount of antioxidant in the composite formulation without blooming

DOI: 10.1021/acsami.5b00993
ACS Appl. Mater. Interfaces 2015, 7, 8156−8165

was dramatically increased using loaded halloysite, while rubber with the same amount of free antioxidant caused severe blooming.

4. CONCLUSION

An aging-resistant styrene−butadiene rubber (SBR) composite was prepared with halloysite clay nanotubes loaded with the antioxidant 4010NA by the addition of 27 wt % of these modified tubes. Silanized halloysite was well dispersed in the SBR matrix. This allowed for the synergistic effect of improved mechanical properties and sustained release of the antioxidant. Encapsulating the antioxidant in the nanotubes allowed for an antioxidant concentration of 3.2 wt % (which otherwise would cause rubber defects) without any indication of surface blooming. The release of 4010NA from halloysite nanotubes in water and nonpolar cyclohexane varies from 4 h to days, but after burying the tube-encapsulated antioxidant into bulk rubber it was extended to more than 9 months (66 wt % was released in the first 5 months). After the incubation at 90 °C for 7 days, the SBR and antioxidant-loaded halloysite composite showed well retained mechanical properties when compared to a control sample. From this research, we conclude that this functionalized halloysite can improve the SBR composite aging resistance without blooming. This approach for functional rubber−halloysite nanocomposites may be extended for other "smart" elastomers, for example, with sustainable antimicrobial rubber protection using halloysite fillers loaded with antiseptics.

■ ASSOCIATED CONTENT

Supporting Information

Figure of the TGA curves of antioxidant in air atmosphere at 90 and 120 °C, and the SEM image and EDS data of the aggregates on the control sample surface. This material is available free of charge via the Internet at http://pubs.acs.org.

■ AUTHOR INFORMATION

Corresponding Authors

*Tel: +86-10-64434860. Fax: +86-10-64433964. E-mail: wangw@mail.buct.edu.cn.
*Tel: +86-10-64434860. Fax: +86-10-64433964. E-mail: zhanglq@mail.buct.edu.cn.
*Tel: +86-10-64434860. Fax: +86-10-64433964. E-mail: ylvov@latech.edu.

Notes

The authors declare no competing financial interest.

■ ACKNOWLEDGMENTS

This work was supported by the National Natural Science Foundation of China (51320105012, 51373010, 50933001, 51221102, 81171682, and 81330043), Beijing Nova Program (Z131102000413015), and Chinese Ministry of Education "Distinguished Overseas Scholar Project". Y.L. acknowledges a partial support by NSF EPS-1003897. Any opinions, findings, and conclusions or recommendations are those of authors and do not necessarily reflect the view of National Science Foundation.

■ REFERENCES

(1) Shelton, J. R. Aging and oxidation of elastomers. *Rubber Chem. Technol.* **1957**, *30*, 1251−1290.
(2) Baldwin, J. M.; Bauer, D. R. Rubber Oxidation and Tire Aging-A Review. *Rubber Chem. Technol.* **2008**, *81*, 338−358.
(3) Garbarczyk, M.; Kuhn, W.; Klinowski, J.; Jurga, S. Characterization of aged nitrile rubber elastomers by NMR spectroscopy and microimaging. *Polymer* **2002**, *43*, 3169−3172.
(4) Mott, P.; Roland, C. Aging of Natural Rubber in Air and Seawater. *Rubber Chem. Technol.* **2001**, *74*, 79−88.
(5) Choi, S. S.; Im, S. H.; Park, J. H.; Kim, J. S. Analysis of Wax Solubility of Rubber Vulcanizates Using Wax Solution in Toluene and Molten Wax. *Polym. Test.* **2009**, *28*, 696−701.
(6) Choi, S. S.; Chung, H. S.; Joo, Y. T.; Yang, K. M.; Lee, S. H. Analysis of Whitening Phenomenon of EPDM Article by Humid Aging. *J. Appl. Polym. Sci.* **2012**, *123*, 2451−2457.
(7) Ismail, M.; Wazzan, A. Evaluation of New Thermal Stabilizers and Antifatigue Agents for Rubber Vulcanizates. *Polym.-Plast. Technol. Eng.* **2006**, *45*, 751−758.
(8) Li, G. Y.; Koenig, J. A Review of Rubber Oxidation. *Rubber Chem. Technol.* **2005**, *78*, 355−390.
(9) Youssef, E.; El-Nashaar, D.; El-Ghaffar, M. A. Evaluation of Itaconic Acid/Aromatic Diamine Adducts as Novel Antioxidants Polymers. Part 1: Evaluation as Antioxidants for Natural Rubber Vulcanizates. *Pigm. Resin Technol.* **2003**, *32*, 219−234.
(10) Li, J.; Wang, S. J.; Liu, H. Y.; Wang, S. K.; You, L. Microencapsulation of Sulfur in Poly (Urea−Formaldehyde). *J. Appl. Polym. Sci.* **2011**, *122*, 767−773.
(11) Jobmann, M.; Rafler, G.; Hensel, M. Microencapsulated Rubber Additives and Method for Production Thereof. Patent US8637592 B2, Jan 28, 2014.
(12) Wang, J.; Chen, Y. Microencapsulation of Intumescent Flame-Retardant Agent: Application to Flame-Retardant Natural Rubber Composite. *J. Appl. Polym. Sci.* **2007**, *104*, 1828−1838.
(13) Wu, G.; An, J.; Tang, X. Z.; Xiang, Y.; Yang, J. A Versatile Approach towards Multifunctional Robust Microcapsules with Tunable, Restorable, and Solvent-Proof Superhydrophobicity for Self-Healing and Self-Cleaning Coatings. *Adv. Funct. Mater.* **2014**, *24*, 6751−6761.
(14) Gao, C. Y.; Möhwald, H.; Shen, J. C. Soluble Microcapsules Assembled Stepwise from Weak Polyelectrolytes Using Acid-Decomposable Cores. *Adv. Mater.* **2003**, *15*, 930−933.
(15) Lu, Y.; Yin, Y.; Xia, Y. Preparation and Characterization of Micrometer-Sized 'Egg Shells'. *Adv. Mater.* **2001**, *13*, 271−274.
(16) Veerabadran, N. G.; Price, R. R.; Lvov, Y. M. Clay Nanotubes for Encapsulation and Sustained Release of Drugs. *Nano* **2007**, *2*, 115−120.
(17) Abdullayev, E.; Lvov, Y. Halloysite Clay Nanotubes as a Ceramic 'Skeleton' for Functional Biopolymer Composites with Sustained Drug Release. *J. Mater. Chem. B* **2013**, *1*, 2894−2903.
(18) Jing, H.; Higaki, Y.; Ma, W.; Wu, H.; Yah, W. O.; Otsuka, H.; Lvov, Y. M.; Takahara, A. Internally Modified Halloysite Nanotubes as Inorganic Nanocontainers for a Flame Retardant. *Chem. Lett.* **2013**, *42*, 121−123.
(19) Abdullayev, E.; Price, R.; Shchukin, D.; Lvov, Y. Halloysite Tubes as Nanocontainers for Anticorrosion Coating with Benzotriazole. *ACS Appl. Mater. Interfaces* **2009**, *1*, 1437−1443.
(20) Yuan, P.; Southon, P. D.; Liu, Z.; Kepert, C. J. Organosilane Functionalization of Halloysite Nanotubes for Enhanced Loading and Controlled Release. *Nanotechnology* **2012**, *23*, 375705.
(21) Lvov, Y.; Abdullayev, E. Functional Polymer-Clay Nanotube Composites with Sustained Release of Chemical Agents. *Prog. Polym. Sci.* **2013**, *38*, 1690−1719.
(22) Vergaro, V.; Abdullayev, E.; Lvov, Y. M.; Zeitoun, A.; Cingolani, R.; Rinaldi, R.; Leporatti, S. Cytocompatibility and Uptake of Halloysite Clay Nanotubes. *Biomacromolecules* **2010**, *11*, 820−826.
(23) Fakhrullina, G. I.; Akhatova, F. S.; Lvov, Y. M.; Fakhrullin, R. F. Toxicity of Halloysite Clay Nanotubes *in vivo*: A *Caenorhabditis elegans* Study. *Environ. Sci.: Nano* **2015**, *2*, 54−59.
(24) Melo, J. D. D.; Barbosa, A. P. C.; Costa, M. C. B.; de Melo, G. N. Encapsulation of Solvent into Halloysite Nanotubes to Promote Self-Healing Ability in Polymers. *Adv. Compos. Mater.* **2014**, 1−13.
(25) Fix, D.; Andreeva, D. V.; Lvov, Y. M.; Shchukin, D. G.; Möhwald, H. Application of Inhibitor-Loaded Halloysite Nanotubes in

DOI: 10.1021/acsami.5b00993
ACS Appl. Mater. Interfaces 2015, 7, 8156−8165

Active Anti-Corrosive Coatings. *Adv. Funct. Mater.* **2009**, *19*, 1720−1727.
(26) Zhao, Y.; Thapa, S.; Weiss, L.; Lvov, Y. Phase Change Heat Insulation Based on Wax-Clay Nanotube Composites. *Adv. Eng. Mater.* **2014**, *16*, 1391−1399.
(27) Du, M.; Guo, B.; Jia, D. Newly Emerging Applications of Halloysite Nanotubes: A Review. *Polym. Int.* **2010**, *59*, 574−582.
(28) Lvov, Y. M.; Shchukin, D. G.; Mohwald, H.; Price, R. R. Halloysite Clay Nanotubes for Controlled Release of Protective Agents. *ACS Nano* **2008**, *2*, 814−820.
(29) Fu, Y.; Liu, L.; Zhang, L.; Wang, W. Highly Conductive One-Dimensional Nanofibers: Silvered Electrospun Silica Nanofibers via Poly(Dopamine) Functionalization. *ACS Appl. Mater. Interfaces* **2014**, *6*, 5105−5112.
(30) Zhou, H.; Wang, H.; Niu, H.; Gestos, A.; Lin, T. Robust, Self-Healing Superamphiphobic Fabrics Prepared by Two-Step Coating of Fluoro-Containing Polymer, Fluoroalkyl Silane, and Modified Silica Nanoparticles. *Adv. Funct. Mater.* **2013**, *23*, 1664−1670.
(31) Carli, L. N.; Daitx, T. S.; Soares, G. V.; Crespo, J. S.; Mauler, R. S. The Effects of Silane Coupling Agents on the Properties of PHBV/Halloysite Nanocomposites. *Appl. Clay Sci.* **2014**, *87*, 311−319.
(32) Raman, V.; Rooj, S.; Das, A.; Stöckelhuber, K.; Simon, F.; Nando, G.; Heinrich, G. Reinforcement of Solution Styrene Butadiene Rubber by Silane Functionalized Halloysite Nanotubes. *J. Macromol. Sci. A* **2013**, *50*, 1091−1106.
(33) Guo, B.; Chen, F.; Lei, Y.; Liu, X.; Wan, J.; Jia, D. Styrene-Butadiene Rubber/Halloysite Nanotubes Nanocomposites Modified by Sorbic Acid. *Appl. Surf. Sci.* **2009**, *255*, 7329−7336.
(34) Abdullayev, E.; Joshi, A.; Wei, W.; Zhao, Y.; Lvov, Y. Enlargement of Halloysite Clay Nanotube Lumen by Selective Etching of Aluminum Oxide. *ACS Nano* **2012**, *6*, 7216−7226.

DOI: 10.1021/acsami.5b00993
ACS Appl. Mater. Interfaces 2015, 7, 8156−8165